PHILOSOPHICAL TRANSACTIONS OF THE ROYAL SOCIETY A MATHEMATICAL, PHYSICAL & ENGINEERING SCIENCES

Constraining large–scale structure theories with the cosmic background radiation

J. Richard Bond and Andrew H. Jaffe

Phil. Trans. R. Soc. Lond. A 1999 **357**, 57-75
doi: 10.1098/rsta.1999.0314

THE ROYAL SOCIETY

Constraining large-scale structure theories with the cosmic background radiation

By J. Richard Bond[1] and Andrew H. Jaffe[2]

[1]*CIAR Cosmology Program, Canadian Institute for Theoretical Astrophysics, 60 St George St., Toronto, ON, Canada M5S 3H8*
[2]*Center for Particle Astrophysics, UC Berkeley, Berkeley, CA 94720, USA*

The case is strong that cosmic microwave background (CMB) and large-scale structure (LSS) observations can be combined to determine the theory of structure formation and the cosmological parameters that define it. We review: the relevant (10+) parameters associated with the inflation model of fluctuation generation and the matter content of the universe; the relation between LSS and primary and secondary CMB anisotropy probes as a function of wavenumber; how COBE constraints on energy injection rule out explosions as a dominant source of LSS; and how current anisotropy band-powers in multipole-space, at levels *ca.* $(10^{-5})^2$, strongly support the gravitational instability theory and suggest the universe could not have reionized too early. We use Bayesian analysis methods to determine what current CMB and CMB+LSS data imply for inflation-based Gaussian fluctuations in tilted ΛCDM, ΛhCDM and oCDM model sequences with cosmological age 11–15 Gyr, consisting of mixtures of baryons, cold 'c' (and possibly hot 'h') dark matter, vacuum energy 'Λ', and curvature energy 'o' in open cosmologies. For example, we find the slope of the initial spectrum is within about 5% of the (preferred) scale-invariant form when just the CMB data are used, and for ΛCDM when LSS data are combined with CMB; with both, a non-zero value of Ω_Λ is strongly preferred (*ca.* $\frac{2}{3}$ for a 13 Gyr sequence, similar to the value from SNIa). The oCDM sequence prefers $\Omega_{\rm tot} < 1$, but is overall much less likely than the flat $\Omega_\Lambda \neq 0$ sequence with CMB + LSS. We also review the rosy forecasts of angular power spectra and parameter estimates from future balloon and satellite experiments when foreground and systematic effects are ignored to show where cosmic parameter determination can go with CMB information alone.

Keywords: inflation; primary cosmic microwave anisotropies; cosmological constant; open universes; COBE; MAP; Planck satellites

1. The relation between CMB and LSS observables

In this section, we first present an overview of the relation between the scales that cosmic microwave background (CMB) anisotropies probe, those that large scale-structure (LSS) observations of galaxy clustering probe, and the scales that are responsible for collapsed object formation in hierarchical models of structure formation, in particular those determining the abundances of clusters and galaxies. We review the basic parameters of amplitude and tilt characterizing the fluctuations in the simplest versions of inflation, but consider progressively more baroque inflation models needing progressively more functional freedom in describing post-inflation fluctuation spectra. We then describe the high precision that has been achieved in

calculations of primary CMB anisotropies (those determinable with linear perturbation theory), and the less precisely calculable secondary anisotropies arising from nonlinear processes in the medium.

(a) *CMB as a probe of early universe physics*

The source of fluctuations to input into the cosmic structure formation problem is likely to be found in early universe physics. We want to measure the CMB (and LSS) response to these initial fluctuations. The goal is to peer into the physical mechanism by which the fluctuations were generated. The contenders for generation mechanism are: (1) 'zero point' quantum noise in scalar and tensor fields that must be there in the early universe if quantum mechanics is applicable; and (2) topological defects which may arise in the inevitable phase transitions expected in the early universe.

From CMB and LSS observations we hope to learn the following: the statistics of the fluctuations, whether Gaussian or non-Gaussian; the mode, whether adiabatic or isocurvature scalar perturbations, and whether there is a significant component in gravitational wave tensor perturbations; the power spectra for these modes, $\mathcal{P}_\Phi(k)$, $\mathcal{P}_{\rm is}(k)$, $\mathcal{P}_{\rm GW}(k)$ as a function of comoving wavenumber $k = 2\pi\bar{a}/\lambda$, with the cosmological scale factor $\bar{a}(t)$ removed from the physical wavelength $\lambda(t)$ and now set to unity. The length unit is h^{-1} Mpc, where h is the Hubble parameter in units of 100 km s^{-1} Mpc^{-1}, i.e. really a velocity unit. Until a few years ago h was considered to be uncertain by a factor of two or so, but is now thought to be between 0.6 and 0.7.

Sample initial and evolved power spectra for the gravitational potential $\mathcal{P}_\Phi(k)$ ($\equiv {\rm d}\sigma_\Phi^2/{\rm d}\ln k$, the RMS power per ${\rm d}\ln k$ band) are shown in figure 1. The (linear) density power spectra, $\mathcal{P}_\rho(k) \propto k^4\mathcal{P}_\Phi(k)$, are also shown in figure 1. (We use $\mathcal{P}(k) = k^3P(k)/(2\pi^2)$ for power spectra, the variance in the fluctuation variable per $\ln k$, rather than the oft-plotted mean-squared fluctuation for mode k, $P(k)$, so $\mathcal{P}_\rho \equiv \Delta^2(k)$ in the notation of Peacock (1997).) As the universe evolves, the initial shape of $\mathcal{P}_\Phi$ (nearly flat or scale invariant) is modified by characteristic scales imprinted on it that reflect the values of cosmological parameters such as the energy densities of baryons, cold and hot dark matter, in the vacuum (cosmological constant), and in curvature. Many observables can be expressed as weighted integrals over k of the power spectra and thus can probe both density parameters and initial fluctuation parameters.

(b) *Cosmic structure and the nonlinear wavenumber*

In hierarchical structure formation models such as those considered here, as the universe evolves $\mathcal{P}_\rho^{1/2}(k)$ grows with time until it crosses unity at small scales, and the first star, forming tiny dwarf galaxies appear ('1st *'), typically at a redshift of about 20. The nonlinear wavenumber $k_{\rm NL}(t)$, defined by

$$\int_0^{k_{\rm NL}} \mathcal{P}_\rho(k)\,{\rm d}\ln k = 1,$$

decreases as the universe expands, leaving in its wake dwarf galaxies (dG), normal galaxies (gal), groups (gps) and clusters (cls), forming from waves concentrated in the k-space bands that their labels cover in figure 1. Equivalent mass scales are given above them.

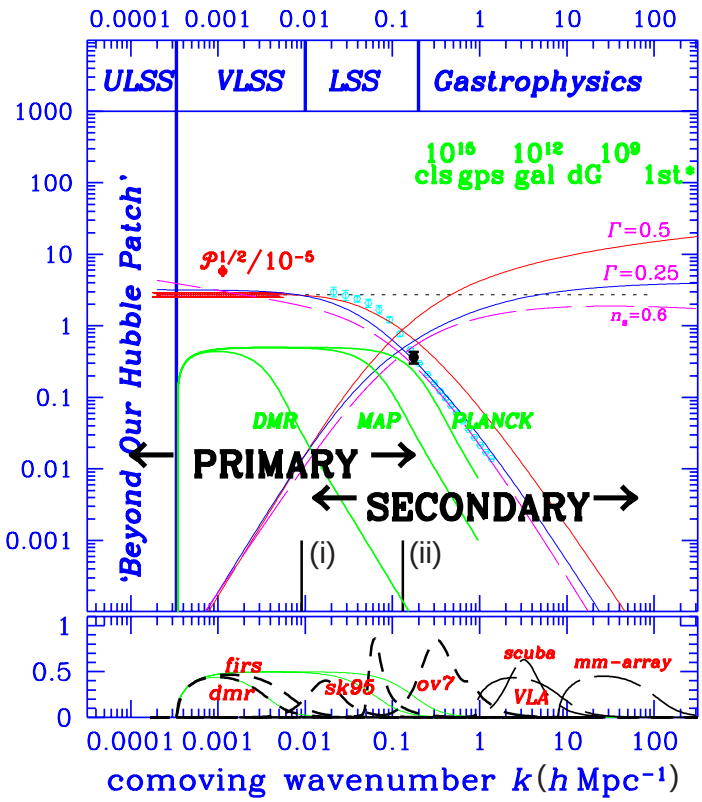

Figure 1. The bands in comoving wavenumber k probed by CMB primary and secondary anisotropy experiments, in particular by the satellites COBE, MAP and Planck, and by LSS observations, are contrasted. The width of the CMB photon-decoupling region ((ii) $\Delta\tau_{\gamma\mathrm{dec}}$) and the sound-crossing radius ((i) $c_{\mathrm{s}}\tau_{\gamma\mathrm{dec}}$) define the effective acoustic peak range for primary anistropies (those involving linear fluctuations). Secondary anisotropies arise only once matter has gone nonlinear. Sample (linear) gravitational potential power spectra (actually $\mathcal{P}_{\Phi}^{1/2}(k)$) are also plotted, and the y-axis values refer to $\mathcal{P}_{\Phi}^{1/2}/10^{-5}$ (which is dimensionless). The horizontal dotted line is the post-inflation scale-invariant power spectrum, which is bent down as the universe evolves by an amount dependent upon the matter content. The hatched region at low k gives the four-year DMR error bar on the Φ amplitude in the COBE regime. The solid data-point in the cluster-band denotes the Φ constraint from the abundance of clusters (for $\Omega_{\mathrm{tot}} = 1$, $\Omega_{\Lambda} = 0$). The open circles are estimates of the linear Φ power from current galaxy clustering data by Peacock (1997). A bias is 'allowed' to (uniformly) raise or lower the shapes to match the observations. The corresponding linear density power spectra, $\mathcal{P}_{\rho}^{1/2}(k)$, are also shown rising to high k. Models shown in this figure are the 'standard' $n_{\mathrm{s}} = 1$ CDM model (labelled $\Gamma = 0.5$ with $\Omega_{\mathrm{nr}} = 1$, $h = 0.5$), a tilted ($n_{\mathrm{s}} = 0.6$, $\Gamma = 0.5$) CDM model and a model with the shape modified ($\Gamma = 0.25$) by changing the matter content of the universe, e.g. $\Omega_{\mathrm{nr}} = 0.36$, $h = 0.7$. The bands at high k associated with object formation (cls, gal, etc.) and the filters showing the bands various CMB experiments probe are discussed in the text.

Scales just below k_{NL} are weakly nonlinear and define the characteristic patterns of filaments connecting clusters, and membranes connecting filaments. Voids are rare density minima which have opened up by gravitational dynamics and merged,

opposite to the equally abundant rare density maxima, the clusters, in which the space collapses by factors of 5–10 and more.

At $k > k_{\rm NL}(t)$, nonlinearities and complications associated with dissipative gas processes can obscure the direct connection to the early universe physics. Most easily interpretable are observables now probing the linear regime, $k < k_{\rm NL}(t_0)$. CMB anisotropies arising from the linear regime are termed primary. As figure 1 shows, these probe three decades in wavenumber, with the high k cutoff defined by the physics at $z \sim 1000$ when CMB photons decoupled, not $k_{\rm NL}$ at that time. Within the LSS band, two important scales for the CMB arise: the sound-crossing distance at photon decoupling, *ca.* $100h^{-1}$ Mpc, and the width of the region over which this decoupling occurs, which is about a factor of 10 smaller, and below which the primary CMB anisotropies are damped. LSS observations of galaxy clustering at low redshift probe a smaller range, but overlap the CMB range. We have hope that $z \sim 3$ LSS observations, when $k_{\rm NL}(t)$ was larger, can extend the range, but gas dynamics can modify the relation between observable and power spectrum in complex ways. Although probes based on catalogues of high redshift galaxies and quasars, and on quasar absorption lines from the intergalactic medium, represent a very exciting observational frontier, it will be difficult for theoretical conclusions about the early universe and the underlying fluctuations to be divorced from these 'gastrophysical' complications. Secondary anisotropies of the CMB (§ 1 *h*), those associated with nonlinear phenomena, also probe smaller scales and the 'gastrophysical' realm.

(*c*) *Probing wavenumber bands with the CMB and LSS*

Although the scales we can probe most effectively are smaller than the size of our Hubble patch (*ca.* $3000h^{-1}$ Mpc), because ultralong waves contribute gentle gradients to CMB observables, we can in fact place useful constraints on the ultralarge scale structure (ULSS) realm 'beyond our horizon'. Indeed current constraints on the size of the universe arise partly from this region and partly from the very large-scale structure (VLSS) region. (For compact spatial manifolds, the wavenumbers have an initially discrete spectrum, and are missing ultralong waves, limited by the size of the manifold.)

The COBE data and CMB experiments with somewhat higher resolution probe the VLSS region very well. Density fluctuations are highly linear in that regime, which is what makes it so simple to analyse. One of the most interesting realms is the LSS realm, in which CMB observations probe exactly the scales that LSS redshift surveys probe. The density fluctuations are linear to weakly nonlinear in this realm, so we can still interpret the LSS observations reasonably well—with one important caveat: galaxies form and shine through complex nonlinear dissipative processes, so how they are distributed may be rather different to how the total mass is distributed. The evidence so far is consistent with this 'bias' being only a linear amplifier of the mass fluctuations on large scales, albeit a different one for different galaxy types. Detailed comparison of the very large CMB and LSS redshift survey results we will get over the next five years should help enormously in determining the statistical nature of the bias.

Because the $\mathcal{P}_\Phi$ of the COBE-normalized sCDM model shown shoots high relative to the cluster data-point, the sCDM model is strongly ruled out. More rigorous discussion of what is compatible with COBE, smaller-angle CMB experiments such

as SK95, the cluster data-point and the shape of the $\mathcal{P}_\Phi$ spectrum as estimated from galaxy clustering data, is given in § 1 *d*. The filter functions plotted for SK95, Planck, etc., show the bands they are sensitive to: multiplying by a k-space $\Delta T/T$ power spectrum gives the variance per $\ln k$ (see, for example, Bond 1996).

(*d*) *The cosmic parameters of structure formation theories*

Even simple Gaussian inflation-generated fluctuations for structure formation have a large number of early universe parameters we would wish to determine (§ 1 *e*): power spectrum amplitudes at some normalization wavenumber $k_{\rm n}$ for the modes present, $\{\mathcal{P}_\Phi(k_{\rm n}), \mathcal{P}_{\rm is}(k_{\rm n}), \mathcal{P}_{\rm GW}(k_{\rm n})\}$; shape functions for the 'tilts' $\{\nu_{\rm s}(k), \nu_{\rm is}(k), \nu_{\rm t}(k)\}$, usually chosen to be constant or with a logarithmic correction, e.g. $\nu_{\rm s}(k_{\rm n}), {\rm d}\nu_{\rm s}(k_{\rm n})/{\rm d}\ln k$. (The scalar tilt for adiabatic fluctuations, $\nu_{\rm s}(k) \equiv {\rm d}\ln\mathcal{P}_\Phi/{\rm d}\ln k$, is related to the usual index, $n_{\rm s}$, by $\nu_{\rm s} = n_{\rm s} - 1$.) The transport problem (§ 1 *g*) is dependent upon physical processes, and hence on physical parameters. A partial list includes the Hubble parameter h, various mean energy densities $\{\Omega_{\rm tot}, \Omega_{\rm B}, \Omega_\Lambda, \Omega_{\rm cdm}, \Omega_{\rm hdm}\}h^2$, and parameters characterizing the ionization history of the universe, e.g. the Compton optical depth $\tau_{\rm C}$ from a reheating redshift $z_{\rm reh}$ to the present. Instead of $\Omega_{\rm tot}$, we prefer to use the curvature energy parameter, $\Omega_k \equiv 1 - \Omega_{\rm tot}$, thus zero for the flat case. In this space, the Hubble parameter, $h = (\sum_j(\Omega_j h^2))^{1/2}$, and the age of the universe, t_0, are functions of the $\Omega_j h^2$. The density in non-relativistic (clustering) particles is $\Omega_{\rm nr} = \Omega_{\rm B} + \Omega_{\rm cdm} + \Omega_{\rm hdm}$†. The density in relativistic particles, $\Omega_{\rm er}$, includes photons, relativistic neutrinos and decaying particle products, if any. $\Omega_{\rm er}$, the abundance of primordial helium, etc., should also be considered as a parameter to be determined. The count is thus at least 17, and many more if we do not restrict the shape of $\mathcal{P}_\Phi(k)$ through theoretical considerations of what is 'likely' in inflation models. Estimates of errors on a smaller nine-parameter inflation set for the MAP and Planck satellites are given in § 2 *e*.

The arena in which CMB theory battles observation is the anisotropy power spectrum in multipole space, as in figures 2 and 3, which show how primary $\mathcal{C}_\ell$ vary with some of these cosmic parameters. Here $\mathcal{C}_\ell \equiv \ell(\ell+1)\langle|(\Delta T/T)_{\ell m}|^2\rangle/(2\pi)$. The $\mathcal{C}_\ell$ are normalized to the four-year dmr$(53 + 90 + 31)$(A + B) data (Bennett *et al.* 1996*a*; Bond 1996; Bond & Jaffe 1997). The arena for LSS theory battling observations is the $\mathcal{P}_\Phi$ of figure 1. (Usually it is $\mathcal{P}_\rho/k^3 \sim k\mathcal{P}_\Phi$ which is plotted.)

For a given model, the early universe $\mathcal{P}_\Phi$ is uniquely related to late-time power spectrum measures of relevance for the CMB, such as the quadrupole $\mathcal{C}_2^{1/2}$ or averages over ℓ-bands B, $\langle\mathcal{C}_\ell\rangle_{\rm B}^{1/2}$, and to LSS measures, such as the RMS density fluctuation level on the $8h^{-1}$ Mpc (cluster) scale, σ_8, so any of these can be used in place of the primordial power amplitudes in the parameter set. In inflation, the ratio of gravitational wave power to scalar adiabatic power is $\mathcal{P}_{\rm GW}/\mathcal{P}_\Phi \approx -\frac{100}{9}\nu_{\rm t}/(1 - \frac{1}{2}\nu_{\rm t})$, with small corrections depending upon $\nu_{\rm s} - \nu_{\rm t}$ (Bond 1994, 1996). If such a relationship is assumed, the parameter count is lowered by one.

(*e*) *Fluctuation freedom in inflation*

Many variants of the basic inflation theme have been proposed, sometimes with radically different consequences for $\mathcal{P}_\Phi(k) \sim k^{1-n_{\rm s}(k)}$, and thus for the CMB sky,

† It is becoming conventional to refer to $\Omega_{\rm nr}$ as $\Omega_{\rm m}$.

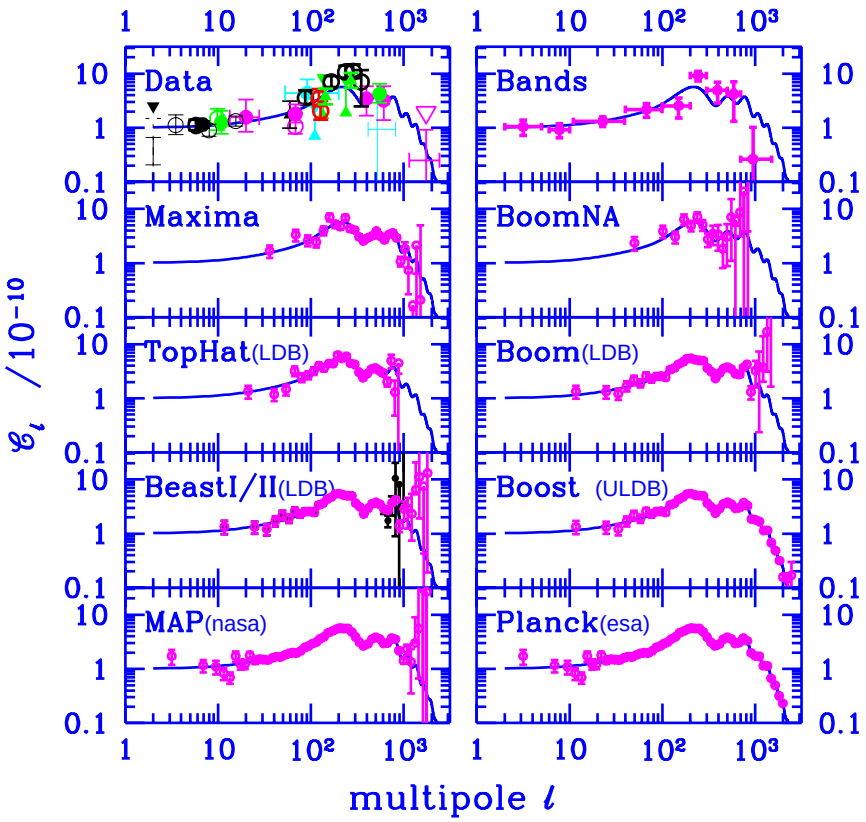

Figure 2. The $\mathcal{C}_\ell$ anisotropy bandpower data for experiments up to summer 1998 are shown in the upper left panel. The data are optimally combined into nine bandpower estimates (with 1σ errors) shown in the upper right panel. To guide the eye an untilted COBE-normalized sCDM model is repeated in all panels. The rest of the panels show forecasts of how accurate $\mathcal{C}_\ell$ will be determined for this model from balloon and satellite experiments, with parameters given in table 1.

which is used in fact to highly constrain the more baroque models. A rank-ordering of inflation possibilities: (1) adiabatic curvature fluctuations with nearly uniform scalar tilt over the observable range, slightly more power to large scales ($0.8 \lesssim n_{\rm s} \lesssim 1$) than 'scale invariance' ($n_{\rm s} = 1$) gives, a predictable non-zero gravity wave contribution with tilt similar to the scalar one, and tiny mean curvature ($\Omega_{\rm tot} \approx 1$); (2) same as (1), but with a tiny gravity wave contribution; (3) same as (1) but with a subdominant isocurvature component of nearly scale-invariant tilt (the case in which isocurvature dominates is ruled out); (4) radically broken scale invariance with weak to moderate features (ramps, mountains, valleys) in the fluctuation spectrum (strong features are largely ruled out); (5) radical breaking with non-Gaussian features as well; (6) 'open' inflation, with quantum tunnelling producing a negatively curved (hyperbolic) space which inflates, but not so much as to flatten the mean curvature ($d_{\rm c} \sim (Ha)^{-1}$, not $\gg (Ha)^{-1}$, where $d_{\rm c} \equiv H_0^{-1}|\Omega_k|^{-1/2}$); (7) quantum creation of compact hyperbolic space from 'nothing' with volume $d_{\rm T}^3$ which inflates, with $d_{\rm T} \sim (Ha)^{-1}$, not $\gg (Ha)^{-1}$, and $d_{\rm T}$ of order $d_{\rm c}$; (8) flat ($d_{\rm c} = \infty$) inflating models which are small tori of scale $d_{\rm T}$ with $d_{\rm T}$ a few $(Ha)^{-1}$ in size. It is quite debatable

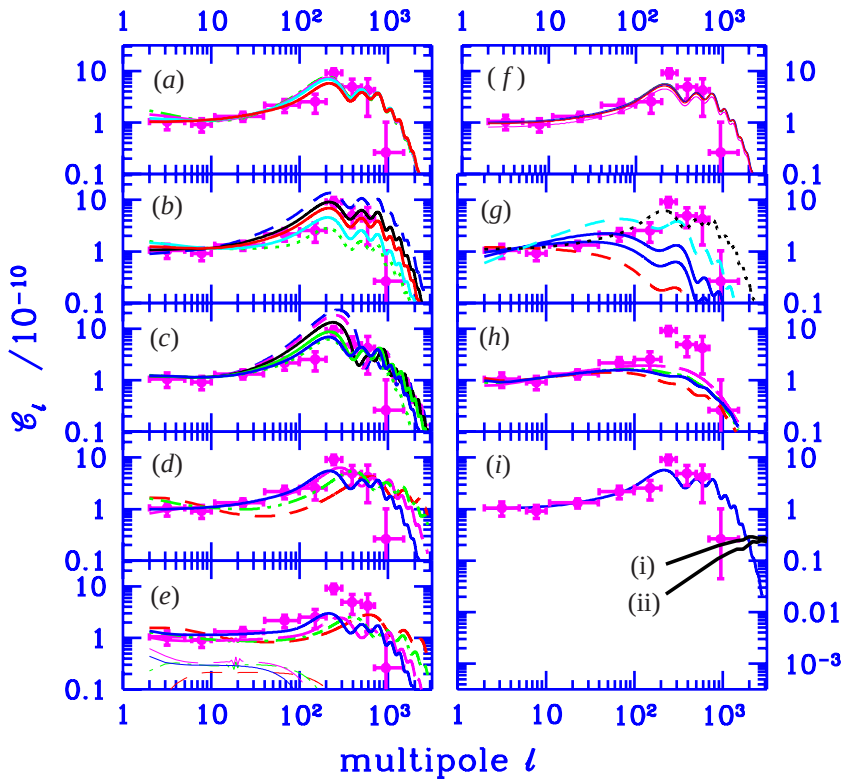

Figure 3. The nine bandpower estimates from current anisotropy data are compared with various 13 Gyr model sequences: (*a*) H_0 from 50–90, Ω_Λ, 0–0.87, for an untilted ΛCDM sequence; (*b*) $n_{\rm s}$ from 0.85–1.25 for the $H_0 = 70$ ΛCDM model ($\Omega_\Lambda = 0.66$); (*c*) $\Omega_{\rm B}h^2$ from 0.003–0.05 for the $H_0 = 70$ ΛCDM model; (*d*) H_0 from 50–65, Ω_k from 0–0.84 for the untilted oCDM sequence; (*e*) the same for a $n_{\rm s} = 0.9$ oCDM sequence, clearly at odds with the data; (*f*) $H_0 = 50$ sequence with neutrino fractions varying from 0.1–0.95; (*g*) shows an isocurvature CDM sequence with positive isocurvature tilts ranging from 0–0.8; (*h*) shows that sample defect $\mathcal{C}_\ell$ from Pen *et al.* (1997) do not fare well compared with the current data; $\mathcal{C}_\ell$ from (Allen *et al.* 1997) are similar. The bottom right panel (*i*) is extended to low values to show the magnitude of secondary fluctuations from the thermal SZ effect for the ΛCDM model ((i) $z = 0$–2; (ii) $z = 0.5$–2). The kinematic SZ $\mathcal{C}_\ell$ is significantly lower. Dusty emission from early galaxies may lead to high signals, but the power is concentrated at higher ℓ, with possibly a weak tail because galaxies are correlated extending into the $\ell \lesssim 2000$ regime.

which of the cases beyond (2) are more or less plausible, with some claims that (4) is supersymmetry inspired, others that (6) is not as improbable as it sounds. Of course, how likely *a priori* the cases (7) and (8) are is completely unknown, but it is the theorists' job to push out the boundaries of the inflation idea and use the data to select what is allowed.

(*f*) *LSS constraints on the power spectrum*

We have always combined CMB and LSS data in our quest for viable models. Figure 1 shows how the two are connected. DMR normalization precisely determines σ_8 for each model considered; comparing with the $\sigma_8 \sim 0.6\Omega_{\rm nr}^{-0.56}$ target value derived

from cluster abundance observations severely constrains the cosmological parameters defining the models. In figure 1, this means the COBE-normalized $\mathcal{P}_\Phi(k)$ must thread the 'eye of the needle' in the cluster band.

Similar constrictions arise from galaxy–galaxy and cluster–cluster clustering observations: the shape of the linear $\mathcal{P}_\Phi$ must match the shape reconstructed from the data. The reconstruction shown is from Peacock (1997). The clustering observations are roughly compatible with an allowed range $0.15 \lesssim \Gamma + \frac{1}{2}\nu_s \lesssim 0.3$, where

$$\Gamma \approx \Omega_{\rm nr} h[\Omega_{\rm er}/(1.68\Omega_\gamma)]^{-1/2} \exp[-(\Omega_B(1+\Omega_{\rm nr}^{-1}(2h)^{1/2}) - 0.06)]$$

characterizes the density transfer function shape. The sCDM model has $\Gamma \approx 0.5$. To get $\Gamma + \frac{1}{2}\nu_s$ in the observed range one can: lower h; lower $\Omega_{\rm nr}$ (ΛCDM, oCDM); raise $\Omega_{\rm er}$, the density parameter in relativistic particles ($1.68\Omega_\gamma$ with three species of massless neutrinos and the photons), e.g. as in τCDM, with a decaying ν of lifetime $\tau_{\rm d}$ and

$$\Gamma \approx 1.08\Omega_{\rm nr} h(1 + 0.96(m_\nu \tau_{\rm d}/{\rm keV\ yr})^{2/3})^{-1/2};$$

raise $\Omega_{\rm B}$; tilt $\nu_s < 0$ (tCDM), for standard CDM parameters, e.g. $0.3 \lesssim n_s \lesssim 0.7$ would be required. Adding a hot dark matter component gives a power spectrum characterized by more than just Γ. In the post-COBE era, all of these models that lower $\Gamma + \frac{1}{2}\nu_s$ have been under intense investigation to see which, if any, survive as the data improve.

(*g*) *Cosmological radiative transport*

Cosmological radiative transfer has a firm theoretical footing. Together with a gravity theory (invariably Einstein's general relativity, but the CMB will eventually be used as a test of the gravity theory) and the transport theory for the other fields and particles present (baryons, hot, warm and cold dark matter, coherent fields, i.e 'dynamical' cosmological 'constants', etc.), we propagate initial fluctuations from the early universe through photon decoupling into the (very) weakly nonlinear phase, and predict *primary anisotropies*, those calculated using either linear perturbation theory (e.g for inflation-generated fluctuations), or, in the case of defects, linear response theory. The sources driving their development are all proportional to the gravitational potential Φ: the 'naive' Sachs–Wolfe effect, $\frac{1}{3}\Phi$; photon bunching and rarefaction (acoustic oscillations), $\frac{1}{4}\delta\rho_\gamma/\rho_\gamma$, responsible for the adiabatic $\frac{1}{3}\delta\rho_{\rm B}/\rho_{\rm B}$ effect and the isocurvature effect; linear-order Thompson scattering (Doppler), $\sigma_{\rm T}\bar{n}_{\rm e}\boldsymbol{v}_{\rm e}\cdot\hat{q}$, with $\sigma_{\rm T}$ the Thomson cross section, $\boldsymbol{v}_{\rm e}$ and $\bar{n}_{\rm e}$ the electron velocity and density, and $\hat{q}$ the photon direction; the (line-of-sight) integrated Sachs–Wolfe effect, *ca.* $2\int_{\rm l.o.s.}\dot{\Phi}$; there are also subdominant anisotropic stress and polarization terms. For primary tensor anisotropies, the sources are the two polarization states of gravity waves, $\frac{1}{2}\dot{h}_{+,\times}$; again there are subdominant polarization terms.

Spurred on by the promise of percent-level precision in cosmic parameters from CMB satellites (§ 2 *e*), a considerable fraction of the CMB theoretical community with Boltzmann transport codes compared their approaches and validated the results to ensure percent-level accuracy up to $\ell \sim 3000$ (Bertschinger *et al.* 1995). An important goal for Bertschinger *et al.* was speed, since the parameter space we wish to constrain has many dimensions. Most groups have solved cosmological radiative transport by evolving a hierarchy of coupled moment equations, one for each ℓ. Although the equations and techniques were in place prior to the COBE discovery for

scalar modes, and shortly after for tensor modes, to get the high accuracy with speed has been somewhat of a challenge. There are alternatives to the moment hierarchy for the transport of photons and neutrinos. In particular, the entire problem of photon transport reduces to integral equations in which the multipoles with $\ell > 2$ are expressed as history-integrals of metric variables, photon-bunching, Doppler and polarization sources. The fastest COMBA-validated code, 'CMBfast', uses this method (Seljak & Zaldarriaga 1996), is publicly available and widely used (e.g. to generate some of the power spectra in figure 3).

(*h*) *Secondary anisotropies*

Although hydrodynamic and radiative processes are expected to play important roles around collapsed objects and may bias the galaxy distribution relative to the mass (*gastrophysics* regime in figure 1), a global role in obscuring the early universe fluctuations by late time generation on large scales now seems unlikely. Not too long ago it seemed perfectly reasonable, based on extrapolation from the physics of the interstellar medium to the pregalactic and intergalactic medium, to suppose hydrodynamical amplification of seed cosmic structure could create the observed universe. The strong limits on Compton cooling from the COBE FIRAS experiment (Fixsen *et al.* 1997), in energy $\delta E_{\rm Compton\ cool}/E_{\rm cmb} = 4y < 6.0 \times 10^{-5}$ (95% CL), constrain the product $f_{\rm exp}R_{\rm exp}^2$ of filling factor $f_{\rm exp}$ and bubble formation scale $R_{\rm exp}$, to values too small for a purely hydrodynamic origin. If supernovae were responsible for the blasts, the accompanying presupernova light radiated would have been much in excess of the explosive energy (more than 100-fold), leading to much stronger restrictions (see, for example, Bond 1996).

Nonetheless, significant 'secondary anisotropies' are expected. These include: linear weak lensing, dependent on the two-dimensional tidal tensor, a projection of the three-dimensional tidal tensor $\partial^2\Phi/\partial x^i\partial x^j$; the Rees–Sciama effect, $2\int_{\rm l.o.s.}\dot{\Phi}_{\rm NL}$, dependent upon the gravitational potential changes associated with nonlinear structure formation; nonlinear Thompson scattering, $\sigma_{\rm T}\delta n_{\rm e}\boldsymbol{v}_{\rm e}\cdot\hat{q}$, dependent upon the fluctuation in the electron density $\delta n_{\rm e}$ as well as $\boldsymbol{v}_{\rm e}$, and responsible for the quadratic-order (Vishniac) effect and the 'kinematic' Sunyaev–Zeldovich (SZ) effect (moving cluster/galaxy effect); the thermal SZ effect, associated with Compton cooling, $\int_{\rm l.o.s.}\psi_K(x)\delta(n_{\rm e}T_{\rm e})$, where $\psi_K(x)$ is a function of $x = E_\gamma/T_\gamma$ passing from -2 on the Rayleigh–Jeans end to x on the Wein end, with a null at $x = 2.83$ (i.e. 1863 μm or 161 GHz); pregalactic or galactic dust emission, *ca.* $\int_{\rm l.o.s.}\psi_{\rm dust}(x_{\rm d})\rho_{\rm d}$, dependent upon the distribution of the dust density $\rho_{\rm d}$ and temperature $T_{\rm d}$ through a function $\psi_{\rm dust}$ of $x_{\rm d} = E_\gamma/T_{\rm d}$.

Secondary anisotropies may be considered as a nuisance foreground to be subtracted to get at the primary anisotropies, but they are also invaluable probes of shorter-distance aspects of structure formation theories, full of important cosmological information. The k-space range they probe is shown in figure 1. The effect of lensing is to smooth slightly the Doppler peaks and troughs of figure 3. $\mathcal{C}_\ell$ from quadratic nonlinearities in the gas at high redshift are concentrated at high ℓ, but for most viable models are expected to be a small contaminant. Thomson scattering from gas in moving clusters also has a small effect on $\mathcal{C}_\ell$ (although it should be measurable in individual clusters). Power spectra for the thermal SZ effect from clusters are larger (Bond & Myers 1996); the example in the bottom panel of figure 3 is for an

untilted $H_0 = 70$ COBE-normalized ΛCDM model, with $\bar{y} \sim 2 \times 10^{-6}(\Omega_{\rm B}h^2/0.025)$, still small compared to the FIRAS constraint. (Here and in the following, when H_0 values are given, the units km s^{-1} Mpc^{-1} are implicit.) Although $\mathcal{C}_\ell^{(\rm SZ)}$ may be small, because the power for such non-Gaussian sources is concentrated in hot or cold spots the signal is detectable, in fact has been for two dozen clusters now at the $\sigma > 5$ level, and indeed the SZ effect will soon be usable for cluster-finding. $\mathcal{C}_\ell$ for a typical dusty primeval galaxy model is concentrated at higher ℓ associated with galaxy sizes, although a small contribution associated with clustering extends into the lower ℓ range. These dusty anisotropies are now observable with instrumentation on sub-millimetre telescopes (e.g. SCUBA on the James Clerk Maxwell Telescope on Mauna Kea, with the k-space filter shown in figure 1).

2. CMB parameter estimation, current and future

(a) *Comparing and combining CMB experiments*

We have progressed from the tens of pixels of early $\Delta T/T$ experiments through thousands for DMR (Bennett *et al*. 1996*a*) and SK95 (Netterfield *et al*. 1997); soon tens of thousands for long duration balloon experiments (LDBs) and eventually millions for the MAP (Bennett *et al*. 1996*b*) and Planck (Bersanelli *et al*. 1996) satellites will be possible. Finding nearly optimal strategies for data projection, compression and analysis which will allow us to disentangle the primary anisotropies from the galactic and extragalactic foregrounds and from the secondary anisotropies induced by nonlinear effects will be the key to realizing the theoretically possible precision on cosmic parameters and so determine the winners and losers in theory space. Particularly powerful is the ability to combine results from different CMB experiments and combine these with LSS and other observations. Application of the same techniques to demonstrate self-consistency and cross-consistency of experimental results is essential for validating conclusions drawn from the end-product of data analysis, e.g. the power spectra in bands as shown in figure 2 and the cosmic parameters they imply.

Current band-powers are shown in the upper panel of figure 2. The first lesson of figures 2 and 3 is that, in broad brush strokes, smaller-angle CMB data (e.g. SP94, SK95, MSAM, MAX) are consistent with COBE-normalized $\mathcal{C}_\ell$ for the untilted inflation-based models. It is possible that some of the results may still include residual contamination, but it is encouraging that completely different experiments with differing frequency coverage are highly correlated and give similar bandpowers, e.g. DMR and FIRS (see, for example, Bond 1996), SK95 and MSAM (Netterfield *et al*. 1997; Knox *et al*. 1998). Lower panels compress the information into nine optimal bandpower estimates derived from all of the current data (see Bond *et al*. (1998*b*) for techniques).

The few data-points below $\ell \lesssim 20$ are mainly from COBE's DMR experiment. Clearly the ℓ-range spanned by DMR is not large enough to fix well the cosmological parameter variations shown in the right panels, but combining CMB anisotropy experiments probing different ranges in ℓ-space improves parameter estimates enormously because of the much extended baseline: it is evident that $n_{\rm s}$ can be reasonably well determined, low Ω open models violate the data, but Ω_Λ cannot be well determined by the CMB alone.

(*b*) *DMR and constraints on ultra large-scale structure*

DMR is fundamental to analyses of the VLSS region and ULSS region, and is the data-set that is the most robust at the current time. The average noise in the $53+90+31$ GHz map is about 20 μK per FWHM beam (*ca.* 7°), and there are about 700 of these resolution elements outside of the galactic disc cut (about 4000 2.6° DMR pixels with 60 μK noise). The signal is about 37 μK per beam: i.e. there is a healthy signal-to-noise ratio. The signal-to-noise for widespread modes (e.g. multipoles with $\ell \lesssim 15$) is even better. Indeed, even with the much higher precision MAP and Planck experiments we do not expect to improve the results on the COBE angular scales greatly because the four-year COBE data have sufficiently large signal-to-noise that one is almost in the cosmic variance error limit (due to realization to realization fluctuations of skies in the theories), which cannot be improved upon no matter how low the experimental noise.

Wiener-filtered maps, shown in figure 4, give the statistically averaged signal given the data and a best-fit signal model. These optimally filtered maps are insensitive to modest variations in the assumed theory. The robustness of features in the maps as a function of frequency and the weak frequency dependence in the bandpowers are strong arguments that what is observed is on the sky with a primary anisotropy origin, made stronger by the compatible amplitudes and positive cross-correlations with the FIRS and Tenerife data-sets.

Recall that the 'beyond our horizon' land in figure 1 is actually partly accessible because long waves contribute gentle gradients to our observables. The DMR data are well suited to probe this regime. Constraints on such 'global parameters' as average curvature from COBE are not very good. Obviously, it is much preferred to use the smaller-angle data on the acoustic peak positions. The COBE data can be used to test whether radical broken scale-invariance results in a huge excess or deficit of power in the COBE k-space band, e.g. just beyond $k^{-1} \sim H_0^{-1}$, but this has not been much explored. The remarkable non-Gaussian structure predicted by stochastic inflation theory would likely be too far beyond our horizon for its influence to be felt. The bubble boundary in hyperbolic inflation models may be closer and its influence shortly after quantum tunnelling occurred could possibly have observable consequences for the CMB. Theorists have also constrained the scale of topology in simple models (figure 4). Bond *et al.* (1997*b*, 1998*a*–*c*) find the torus scale is $\frac{1}{2}d_{\rm T} > 1.1(2H_0^{-1}) = 6600h^{-1}$ Mpc from DMR for flat equal-sided 3-tori at the 95% confidence limit, slightly better than other groups find since full map statistics were used. The constraint is not as strong if the repetition directions are asymmetric, greater than $0.7(2H_0^{-1})$ for 1-tori from DMR. It is also not as strong if more general topologies are considered, e.g. the large class of compact hyperbolic topologies (Bond *et al.* 1997*b*, 1998*a*–*c*; Cornish *et al.* 1998; Levin *et al.* 1997, 1998).

(*c*) *Cosmic parameters from all current CMB data*

We have undertaken full Bayesian statistical analysis of the four-year DMR (Bennet *et al.* 1996*a*), SK94–95 (Netterfield *et al.* 1997) and SP94 (Gundersen *et al.* 1995) data-sets, taking into account all correlations among pixels in the data and theory (Bond & Jaffe 1997). Other experiments available up to March 1998 were included by using their bandpowers as independent points with the Gaussian errors shown in figure 2. We have shown this approximate method works reasonably well

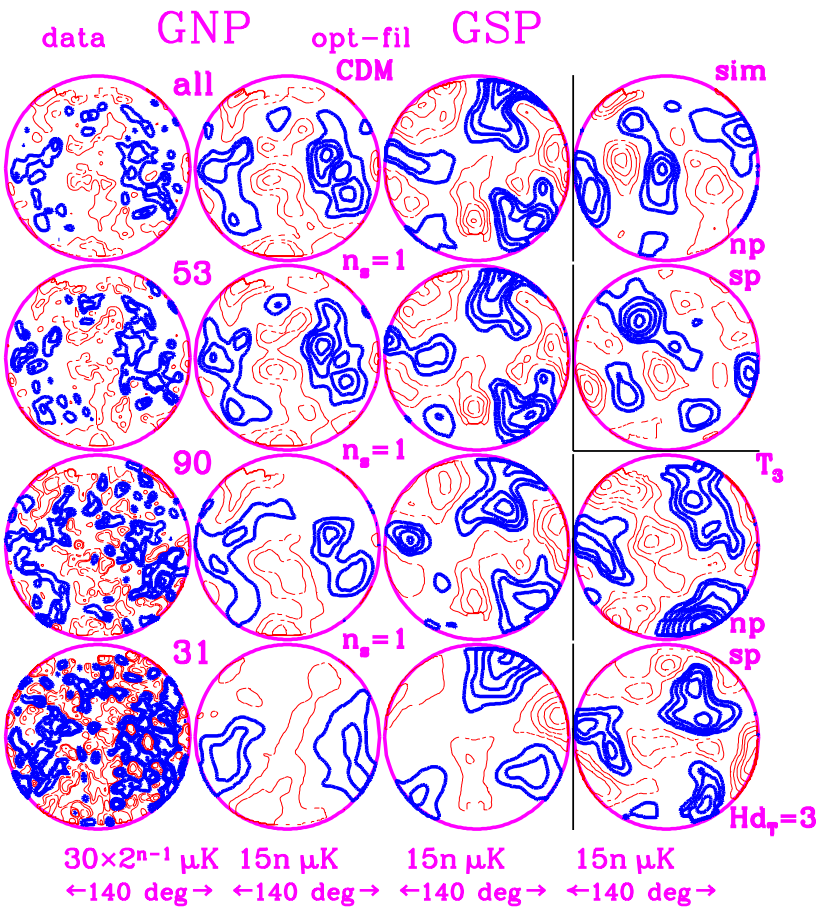

Figure 4. The first column shows unfiltered 140° diameter dmr A + B maps centred on the North Galactic Pole, the second shows them after Wiener-filtering (with monopole, dipole and quadrupole removed), the third shows the South Pole version, with the nth contour as noted and negative contours heavier than positive contours. The Wiener maps use a model which fits the correlation function and amplitude of the DMR data (specifically, the $n_s = 1$ sCDM model was used, but was insensitive to even rather significant variations). The maps have been smoothed by a 1.7° Gaussian filter. *all* is 53+90+31A+B. Although higher noise results in filtering on greater angular scales, the large-scale features of all maps are the same. This is also borne out by detailed statistical comparisons map to map. The last column shows some theoretical realizations, after optimal filtering. The first two rows are the NGP and SGP for an $n_s = 1$ CDM model. The lower two rows are for a 3-torus topology, with repetition length $d_T = 9000h^{-1}$ Mpc, 1.5 times the horizon radius, in all three directions, a model strongly ruled out because of the high degree of positive correlation between the northern and southern hemispheres that the periodicity induces (Bond *et al*. 1998*a*–*c*). Highly correlated patterns also exist for small compact hyperbolic models and lead to constraints on manifold size.

by comparing results derived for DMR + SP94 + SK95 with the full analysis with those using just their bandpowers (Jaffe *et al*. 1997). We have also shown that a significant improvement in accuracy is possible if instead of the average and 1σ limits on the experimental bandpowers $\mathcal{C}_B$ or on $\mathcal{C}_B^{1/2}$, one uses $\ln(\mathcal{C}_B + x_B)$, where x_B is related to the noise of the experiment (Bond *et al*. 1998*b*). This includes some of the

major non-Gaussian deviations in the bandpower likelihood functions; results using this more accurate approach, and incorporating the very recent CAT98 and QMAP data, will be reported elsewhere (Bond *et al*. 1998*c*). Other groups have also calculated parameter constraints using the $\mathcal{C}_{\rm B}^{1/2}$ bandpower approach (see, for example, Lineweaver & Barbosa 1997; Hancock & Rocha 1997; Lineweaver 1998).

With current errors in the data, simultaneously exploring the entire parameter space of § 1 *d* is not useful, so we restricted our attention to various subregions of $\{\Omega_{\rm B}h^2, \Omega_{\rm cdm}h^2, \Omega_{\rm hdm}h^2, \Omega_k h^2, \Omega_\Lambda h^2, \nu_{\rm s}, \nu_{\rm t}, \sigma_8\}$, such as $\{\sigma_8, n_{\rm s}, h \mid \text{fixed } t_0, \Omega_{\rm B}h^2\}$, where $\Omega_k = 0$ and Ω_Λ is a function of ht_0, or $\Omega_\Lambda = 0$ and $\Omega_k > 0$ is a function of ht_0. The age of the universe, t_0, was chosen to be 11, 13 or 15 Gyr. A recent estimate for globular cluster ages with the Hipparcos correction is 11.5 ± 1.3 Gyr (Chaboyer *et al*. 1998), with perhaps another Gyr to be added associated with the delay in globular cluster formation, so 13 Gyr is a good example. We considered the ranges $0.5 \leqslant n_{\rm s} \leqslant 1.5$, $0.43 \leqslant h \leqslant 1$ and $0.003 \leqslant \Omega_{\rm B}h^2 \leqslant 0.05$. The old 'standard' nucleosynthesis estimate was $\Omega_{\rm B}h^2 = 0.0125$, but the preferred one is now 0.025. We assumed reheating occurred sufficiently late to have a negligible effect on $\mathcal{C}_\ell$, although this is by no means clear. $\mathcal{C}_\ell$ for sample restricted parameter sequences are shown in figure 3. We made use of signal-to-noise compression of the data (by factors of three) in order to make the calculations of likelihood functions such as $\mathcal{L}(\sigma_8, n_{\rm s}, h \mid \text{fixed } t_0, \Omega_{\rm B}h^2)$ more tractable (without loss of information or accuracy).

The $n_{\rm s}$ constraints are quite good. If σ_8 is marginalized for the tilted ΛCDM sequence with $H_0 = 50$, with DMR only, the primordial index is $n_{\rm s} = 1.02^{+0.23}_{-0.25}$ with no gravity waves and $\nu_{\rm t} = 0$, and $1.02^{+0.23}_{-0.18}$ with gravity waves and $\nu_{\rm t} = \nu_{\rm s}$, rather encouraging for the nearly scale-invariant models preferred by inflation theory. Because the gravitational potential changes at late time with $\Lambda \neq 0$, the integrated Sachs–Wolfe effect gives more power in $\mathcal{C}_\ell$ at small ℓ, so the preferred $n_{\rm s}$ steepens to compensate. When Λ is marginalized in the 13 Gyr tilted ΛCDM sequence, $n_{\rm s} = 1.17 \pm 0.31$ is obtained. For this sequence, when all of the current CMB data are used we get $1.02^{+0.05}_{-0.03}$ for $H_0 = 50$ (and $\Omega_\Lambda = 0$, the tilted sCDM model sequence) and $1.00^{+0.04}_{-0.04}$ for $H_0 = 70$ (and $\Omega_\Lambda = 0.66$). Marginalizing over H_0 (i.e. Λ) gives $1.01^{+0.05}_{-0.04}$ with gravity waves included, $0.98^{+0.08}_{-0.06}$ if they are not. The marginalized 13 Gyr tilted oCDM sequence gives $1.00^{+0.05}_{-0.05}$.

H_0 and Ω_Λ for fixed age are not that well determined by the CMB data alone, as can be seen from the dotted lines in figure 5. After marginalizing over all $n_{\rm s}$, we get $H_0 < 75$ at 1σ, but effectively no constraint at 2σ. The strong dependence of the position of the acoustic peaks on Ω_k means that the oCDM sequence is better restricted: $\Omega_{\rm tot} \sim 0.7$ is preferred; for the 13 Gyr sequence this gives $H_0 \approx 53$ and for the 11 Gyr sequence $H_0 \approx 65$.

Calculations of defect models (e.g. strings and textures) give $\mathcal{C}_\ell$ that do not have the prominent peak that the data seem to indicate (Pen *et al*. 1997; Allen *et al*. 1997).

(*d*) *Cosmic parameters from current LSS plus CMB data*

Combining LSS and CMB data gives more powerful discrimination among the theories, as figure 1 illustrates visually and figure 5 shows quantitatively. The approach we use here and in Bond & Jaffe (1997) to add LSS information to the CMB likelihood functions is to design prior probabilities for $\Gamma + \frac{1}{2}\nu_{\rm s}$ and $\sigma_8\Omega_{\rm nr}^{0.56}$, reflecting the current observations, but with flexible and generous non-Gaussian and asymmetric

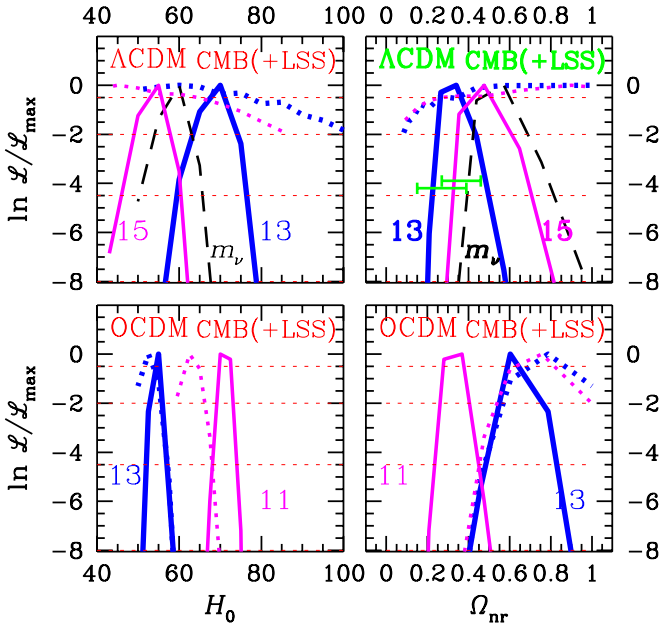

Figure 5. Likelihood curves for fixed-age ΛCDM and oCDM sequences, marginalized over σ_8 and n_s. A Gaussian approximation to the likelihood places 1,2,3σ at the horizontal dashed lines. The 1σ ranges are explicitly given in the text. The dotted curves are for CMB only, solid for CMB + LSS. The right panels are equivalent to the left, but translated to Ω_{nr} ($1-\Omega_\Lambda$ for ΛCDM, Ω_{tot} for oCDM). The curves shown are for no GW, but there is little difference if GW are included. The sequence labelled m_ν is for the 13 Gyr ΛhCDM sequence with a fixed $\Omega_{m_\nu}/\Omega_{nr}$ ratio of 0.2, and two degenerate neutrino species. Even this case slightly favours a non-zero Ω_Λ. Note that the CMB data alone slightly favour a value of $\Omega_{tot} < 1$. The absolute likelihood for the CMB + LSS data strongly favours the ΛCDM over the oCDM sequences. When just the fully analysed DMR + SK95 + SP94 data are used with LSS, the marginalized results for ΛCDM are remarkably similar, with the long baseline between DMR and SK95 fixing the freedom in n_s (although values of n_s about 1.1 are now preferred). When only DMR is used along with LSS, n_s is not nailed down, and the resulting freedom implies $\Omega_{nr} = 1$ models are not disfavoured. The horizontal error bars in the upper right panel show the 1σ range of Ω_{nr} for $\Omega_{nr}+\Omega_\Lambda = 1$ models inferred from the supernova Ia observations of Perlmutter *et al.* (1998) (upper) and Reiss *et al.* 1998 (lower).

forms to ensure the priors can encompass possible systematic problems in the LSS data. For example, our choice for $\sigma_8\Omega_{nr}^{0.56}$ was relatively flat over the 0.45–0.65 range. (Explicitly we used $0.55^{+0.02+0.15}_{-0.02-0.08}$, with the two error bars giving a Gaussian and a top-hat error so that the net result is generously flat over the total $\pm1\sigma$ range. For $\Gamma+\frac{1}{2}\nu_s$, we used $0.22^{+0.07+0.08}_{-0.04-0.07}$. Using the Peacock (1997) reconstructed linear power spectrum shown in figure 1 would give more stringent constraints for the shape (see, for example, Gawiser & Silk 1998).)

Using all of the current CMB data and the LSS priors, for the 13 Gyr ΛCDM sequence with gravity waves included, we get $n_s = 1.00^{+0.05}_{-0.03}$ and $H_0 = 72 \pm 3$ ($\Omega_\Lambda \approx 0.7$), respectively, when H_0 and n_s are marginalized; with no gravity waves, $0.96^{+0.07}_{-0.05}$ and $H_0 = 70 \pm 3$ are obtained; and for an ΛhCDM sequence, with a fixed ratio $\Omega_{hdm}/\Omega_{nr} = 0.2$ for two degenerate massive neutrino species, $n_s \approx 0.97^{+0.02}_{-0.02}$

and $H_0 \approx 57^{+5}_{-3}$ are obtained, revealing a slight preference for $\Omega_\Lambda \sim 0.3$. For the 15 Gyr ΛCDM sequence, the tilts remain nearly scale invariant and Ω_Λ near 0.6: $0.98^{+0.04}_{-0.03}$ and $H_0 = 57 \pm 3$ ($\Omega_\Lambda \approx 0.6$) with gravity waves, $0.95^{+0.05}_{-0.05}$ and 54 ± 3 ($\Omega_\Lambda \approx 0.5$) without.

For the 13 Gyr oCDM sequence, the likelihood peak for the CMB + LSS data is shifted relative to using the CMB data alone because the best fit CMB-only models have σ_8 too low compared with the cluster abundance requirements. Although the $H_0 \approx 54^{+1}_{-1}$ value ($\Omega_{\rm tot} \approx 0.6$) is close to the CMB-only value, the maximum likelihood is significantly below the ΛCDM value. H_0 is larger for the 11 Gyr oCDM sequence, but $\Omega_{\rm tot}$ is about the same, and the likelihood is still low.

Should these small error bars be taken seriously? It seems unlikely that σ_8 from cluster abundances will change much; and, as we have seen, the DMR results are quite robust. Although largely driven by just the DMR + LSS results, the smaller-angle CMB results lock in the tilt, and, as the CMB data improve, some adjustment might occur, but not a drastic one unless we have made a major misinterpretation in the nature of the CMB signals observed at intermediate angles.

If we were to marginalize over t_0 as well, it is clear that H_0 would not be as well determined, but $n_{\rm s}$ and either Ω_k or Ω_Λ would be. If the parameter space is made even larger, near degeneracies among some cosmic parameters become important for CMB data alone, and these are only partly lifted by the LSS data (see, for example, Efstathiou & Bond 1998). In particular, this restricts the ultimate accuracy that can be achieved in the simultaneous determination of Ω_k and Ω_Λ. This will become an issue when the quality of the CMB data improves, as described in the next subsection, but for now one must bear in mind the constrained space used when interpreting the current precision quoted on parameter estimation.

(*e*) *Cosmic parameters from the CMB future*

The expected error bars on the power spectrum from MAP and Planck (Bond *et al*. 1998*a*; Bond *et al*. 1997*a*, hereafter BET) shown in figure 2 illustrate that even quite small differences in the theoretical $\mathcal{C}_\ell$ and thus the parameters can be distinguished. Quite an industry has developed forecasting how well future balloon experiments (Maxima, Boomerang, ACE, Beast, Top Hat), interferometers (VSA, CBI, VCA) and especially the satellites MAP and Planck could do in measuring the radiation power spectrum and cosmological parameters if foreground contamination is ignored (Knox 1995; Jungman *et al*. 1996; BET; Zaldarriaga *et al*. 1997; White *et al*. 1997). Forecasts like these were quite influential in making the case for MAP and Planck.

Table 2 gives some examples of what can be obtained using only CMB data (BET). The experimental parameters chosen are given in table 1. The durations chosen were appropriate for the types of experiments, e.g. about a week for long-duration balloon experiments and about two years for satellite experiments. The temperature anisotropies were assumed to be Gaussian-distributed, and among the 17+ parameters of § 1 *d*, a restricted nine-parameter space was used: five densities, $\{\Omega_{\rm B}; \Omega_{\rm nr}, \Omega_{\rm hdm}, \Omega_k, \Omega_\Lambda\}h^2$; the Compton depth $\tau_{\rm C}$; the scalar tilt; $n_{\rm s}$; the total bandpower for the experiment, $\langle \mathcal{C}_\ell \rangle_{\rm B}$, in place of $\mathcal{P}_\Phi(k_{\rm n})$; and the ratio of tensor to scalar quadrupole powers, $r_{\rm ts} \equiv \mathcal{C}_2^{\rm (T)}/\mathcal{C}_2^{\rm (S)}$, in place of $\nu_{\rm t}$. Just like $\mathcal{P}_{\rm GW}/\mathcal{P}_\Phi$, $r_{\rm ts}$ is a sensitive function of $\nu_{\rm t}$, but also depends on $\nu_{\rm s} - \nu_{\rm t}$, Ω_Λ, etc. (Bond 1996). In this space, recall that $h^2 = \sum_j (\Omega_j h^2)$ is a dependent quantity.

Table 1.

(The noise is per FWHM pixel, in μK; max is Maxima, TH is TopHat, and Bst is Beast, which also has a 30 GHz channel (26′, 53 μK) included in the analysis. Bm is Boomerang, which also has 220 and 430 GHz channels not included in the analysis. The North America test flights covered 0.008 and 0.003 of the sky, and had FWHM of 35′ and 19′, respectively. Boost is a bolometer-based version of Beast that is an example of an ultra-long duration balloon experiment, of order 100 days, with channels at 100 GHz (9′, 17 μK), 140 GHz (6′, 24 μK), (4′, 37 μK), covering 0.07 of the sky, with $\ell_{\rm cut} \approx 6$. The Planck numbers are for the HFI channels; a 350 GHz (4′, 43 μK) was also included in the analysis. See BET for the three channels of LFI used.)

	max	TH	BstI	II	Bm	Bm	MAP			Pl		
$f_{\rm sky}$	0.01	0.028	0.067	0.067	0.02	0.02	0.67	0.67	0.67	0.67	0.67	0.67
$\ell_{\rm cut}$	20	12	6	6	12	12	2	2	2	2	2	2
ν	all	all	40	90	90	150	90	60	40	100	150	220
$\theta_{\rm FWHM}$	12	20	19	9	20	12	13	18	32	14.5	10	6.6
σ_{Npix}	24	18.4	31	100	21	35	34	25	14	3.4	3.6	3.2

Except for the integrated Sachs–Wolfe effect at low ℓ, the angular pattern of CMB anisotropies now is a direct map of the projected spatial pattern at redshift *ca.* 100, dependent upon the cosmological angle–distance relation, which is constant along a line relating $\Omega_k h^2$ and $\Omega_\Lambda h^2$ for fixed $\Omega_{\rm nr} h^2$. This defines a near-degeneracy between Ω_k and Ω_Λ, broken only at low ℓ where the large cosmic variance precludes accurate determination of both parameters simultaneously (see, for example, BET; Zaldarriaga *et al.* 1997; Efstathiou & Bond 1998; Eisenstein *et al.* 1998). Other cosmological observables are needed to break this degeneracy. A good example is type I supernovae. If they are assumed to be 'standard candles', then their degeneracy is along lines of equal luminosity–distance, which is sufficiently different from the equal angle–distance lines to allow good separate determination.

If the polarization power spectrum can be measured with reasonable accuracy, errors on some parameter such as $r_{\rm ts}$ would improve (Zaldarriaga *et al.* 1997). However, the polarization power spectrum is about 100 times lower than the total anisotropy, and the gravity-wave-induced polarization is substantially tinier than this at the low ℓ needed for $r_{\rm ts}$ improvement. We do not know if the foreground polarization will hopelessly swamp this signal.

Error forecasts do depend upon the correct underlying theory. In table 2, untilted sCDM was chosen as the target model, but the values shown are indicative of what is obtained with other targets (BET). The third column gives errors forecasted for balloon experiments, the bolometer-based TopHat, Boomerang, and MAXIMA and the HEMT-based Beast. (URLs to home pages are given in the references.) ℓ-cuts were included to reflect the limited sky coverage these experiments will have. Adding DMR to extend the ℓ-baseline diminishes the forecasted errors.

We adopt the current beam sizes and sensitivities for MAP and Planck used in BET, improvements over the original proposal values. Of the five HEMT channels for MAP, BET assumed that the three highest frequency channels, at 40, 60 and 90 GHz, will be dominated by the primary cosmological signal (with 30 and 22 GHz channels partly contaminated by bremsstrahlung and synchrotron emission). MAP

Table 2. *Sample idealized MAP and Planck parameter error forecasts, for a nine-parameter inflation family of models, with standard CDM the 'target model' (see BET for methods)*

($\Omega_\Lambda h^2$ is determined with $\Omega_k h^2$ fixed, and $\Omega_k h^2$ is determined with $\Omega_\Lambda h^2$ fixed, because of the angle-distance near-degeneracy (see, for example, Efstathiou & Bond 1998); the other parameters are insensitive to fixing either, or neither. The ranges for H_0, $\Omega_{\rm B}h^2$ are absolute, but the errors are relative. The forecasted errors obviously represent a great leap forward from current errors and from what is conceivable with non-CMB probes. Amplitude parameters are highly correlated with $\tau_{\rm C}$, but this can be partly broken when other information is included, e.g. on the abundance of clusters. The third column is an optimistic forecast of what one can do with balloons by combining MAXIMA, TopHat, Boomerang and BeastI with DMR (see figure 2). TopHat, Boomerang, and BeastI would be long-duration balloon flights, lasting about a week over the Antarctic. The parameters used are given in table 1. It is unclear that systematics will be sufficiently small for the LDB experiments to fulfil this promise.)

parameter	current range	MaxTHBoom +BeastI + dmr	MAP	Planck LFI	Planck HFI
$f_{\rm sky}$		0.07	0.67	0.67	0.67
$\delta n_{\rm s}$	(0.5–1.5)	0.07	0.04	0.01	0.006
δr_{ts}	(0–1)	0.55	0.24	0.13	0.09
$\delta\Omega_b h^2/\Omega_b {\rm h_0}^2$	(0.01–0.03)	0.11	0.05	0.016	0.006
$\delta\Omega_m h^2/{\rm h_0}^2$	(0.2-1)	0.20	0.10	0.04	0.02
$\delta\Omega_\Lambda h^2/{\rm h_0}^2$	(0–0.8)	0.46	0.28	0.14	0.05
$\delta\Omega_{hdm} h^2/{\rm h_0}^2$	(0–0.3)	0.14	0.05	0.04	0.02
τ_C	(0.01–1)	0.26	0.19	0.18	0.16
$\delta h/h$	(40–80)	0.15	0.11	0.06	0.02
$\delta\Omega_k h^2/{\rm h_0}^2$	(0.2–1.5)	0.06	0.04	0.02	0.007
	orthogonal parameter combinations within ε				
$\varepsilon < 0.01$	0/9	2/9	3/9	3/9	5/9
$\varepsilon < 0.1$	1/9	6/9	6/9	6/9	7/9

also assumes two years of observing. For Planck, BET used 14 months of observing the 100, 65 and 44 GHz channels for the HEMT-based LFI (but not the 30 GHz channel), and the 100, 150, 220 and 350 GHz channels for the bolometer-based HFI (but not the dust-monitoring 550 and 850 GHz channels). The highest resolution for MAP is $13'$ FWHM, the highest for Planck is $4'$.

These idealized error forecasts do not take into account the cost of separating the many components expected in the data, in particular galactic and extragalactic foregrounds, but there is currently optimism that the galactic foregrounds at least may not be a severe problem (see, for example, Bersanelli *et al.* 1996), although low-frequency emission near 100 GHz by small spinning dust grains (Leitch *et al.* 1997; Draine & Lazarian 1998) may emerge as a new significant source. There is more uncertainty about the extragalactic contributions in the submm and radio.

Although we may forecast wonderfully precise power spectra and cosmic parameters for the simplest inflation models in table 2, once we consider the more baroque models with multifeatured spectra the precision drops (see, for example, Souradeep

et al. 1998). Given that all of our CMB and LSS observations actually access only a very small region of the inflation potential, imposing theoretical 'prior' costs on highly exotic post-inflation shapes over the observable bands is reasonable. Nonetheless, if the phenomenology ultimately does teach us that non-baroque inflation and defect models fail, the CMB and LSS data will be essential for guiding us to a new theory of fluctuation generation.

We thank George Efstathiou, Lloyd Knox, Dmitry Pogosyan and Tarun Souradeep for enjoyable collaborations on a number of the projects highlighted in the text.

References

Allen, B., Caldwell, R. R., Dodelson, S., Knox, L., Shellard, E. P. S. & Stebbins, A. 1997 Preprint, astro-ph/9704160.

Beast home page. http://www.deepspace.ucsb.edu/research/Sphome.html

Bennett, C. L., Banday, A. J., Górski, K. M., Hinshaw, G., Jackson, P., Keegstra, P., Kogut, A., Smoot, G. F., Wilkinson, D. T. & Wright, E. L. 1996*a* *Astrophys. J. Lett.* **464**, 1.

Bennett, C. L. (and 12 others) 1996*b* MAP home page. http://map.gsfc.nasa.gov

Bersanelli, M. (and 12 others) 1996 COBRAS/SAMBA. The phase A study for an ESA M3 mission. ESA report D/SCI(96)3. Planck home page. http://astro.estec.esa.nl/SA-general/Projects/Planck

Bond, J. R. 1994 In *Relativistic cosmology. Proc. 8th Nishinomiya-Yukawa Memorial Symp.* (ed. M. Sasaki), pp. 23–55. Tokyo: Universal Academy Press.

Bond, J. R. 1996 Theory and observations of the cosmic background radiation. In *Cosmology and large-scale structure, Les Houches Session LX, August 1993* (ed. R. Schaeffer). New York: Elsevier.

Bond, J. R. & Jaffe, A. 1997 In *Microwave background anisotropies. Proc. XXXI Rencontre de Moriond* (ed. F. R. Bouchet), pp. 197. Paris: Edition Frontières.

Bond, J. R. & Myers, S. 1996 *Astrophys. J. Suppl.* **103**, 1–79.

Bond, J. R., Efstathiou, G. & Tegmark, M. 1997*a* *Mon. Not. R. Astr. Soc.* **291**, L33.

Bond, J. R., Pogosyan, D. & Souradeep, T. 1997*b* *Proc. 18th Texas Symp. on Relativistic Astrophysics* (ed. A. Olinto, J. Frieman & D. Schramm), pp. 297–299. Singapore: World Scientific.

Bond, J. R., Jaffe, A. H. & Knox, L. 1998*a* *Phys. Rev.* D **57**, 2117.

Bond, J. R., Jaffe, A. H. & Knox, L. 1998*b* *Astrophys. J.* astro-ph/9808264. (In the press.)

Bond, J. R., Pogosyan, D. & Souradeep, T. 1998*c* *Class. Quant. Grav.* **15**, 2671.

Boomerang home page: http://astro.caltech.edu/ mc/boom/boom.html

Chaboyer, B., Demarque, P., Krauss, L. M. & Kernan, P. J. 1998 *Astrophys. J.* **494**, 96.

Bertschinger, E. (and 21 others) 1995 *ITP Workshop on Cosmic Radiation Backgrounds and the Formation of Galaxies (COMBA), Santa Barbara, CA*.

Cornish, N. J., Spergel, D. N. & Starkman, G. D. 1998 *Class. Quant. Grav.* **15**, 2657.

Draine, B. T. & Lazarian, A. 1998 *Astrophys. J. Lett.* **494**, 19.

Efstathiou, G. & Bond, J. R. 1998 *Mon. Not. R. Astr. Soc.* (In the press.)

Eisenstein, D. J., Hu, W. & Tegmark, M. 1998 Preprint, astro-ph/9807130.

Fixsen, D. J., Cheng, E. S., Gales, J. M., Mather, J. C., Shafer, R. A. & Wright, E. L. 1997 *Astrophys. J.* **473**, 576.

Gawiser, E. & Silk, J. 1998 *Science* **280**, 1405.

Gundersen, J. O. (and 11 others) 1995 *Astrophys. J. Lett.* **443**, 57–60.

Hancock, S. & Rocha, G. 1997 In *Proc. XVIth Moriond meeting, Microwave Background Anisotropies* (ed. F. R. Bouchet *et al*.). Gif-Sur-Yvette: Editions Frontières.

Jaffe, A. H., Knox, L. & Bond, J. R. 1997 *Proc. 18th Texas Symp. on Relativistic Astrophysics* (ed. A. Olinto, J. Frieman and D. Schramm), pp. 273–275. Singapore: World Scientific.

Jungman, G., Kamionkowski, M., Kosowsky, A. & Spergel, D. N. 1996 *Phys. Rev.* D **54**, 1332.

Knox, L. 1995 *Phys. Rev.* D **52**, 4307–4318.

Knox, L., Bond, J. R., Jaffe, A. H., Segal, M. & Charbonneau, D. 1999 *Phys. Rev.* D **58**. (In the press.)

Leitch, E. M., Readhead, A. C. S., Pearson, T. J. & Myers, S. T. 1997 *Astrophys. J. Lett.* **486**, 23.

Levin, J. J., Barrow, J. D., Bunn, E. F. & Silk, J. 1997 *Phys. Rev. Lett.* **79**, 974.

Levin, J. J., Scannapieco, E. & Silk, J. 1998 *Class. Quant. Grav.* **15**, 2689.

Lineweaver, C. 1999 In *Proc. The Cosmic Microwave Background and the Planck Surveyor Mission, 22–26 June 1998, Santander, Spain.* Preprint, astro-ph/9810334.

Lineweaver, C. & Barbosa, D. 1998 *Astrophys. J. Lett.* **496**, 624.

MAXIMA home page. http://physics7.berkeley.edu/group/cmb/gen.html.

Netterfield, C. B., Devlin, M. J., Jarosik, N., Page, L. & Wollack, E. J. 1997 *Astrophys. J.* **474**, 47.

Peacock, J. A. 1997 *Mon. Not. R. Astr. Soc.* **284**, 885.

Pen, Ue-Li, Seljak, U. & Turok, N. 1997 Preprint, astro-ph/9704165.

Perlmutter, S. (and 31 others) 1998 Preprint, astro-ph/9812133.

Reiss, A. G. (and 19 others) 1998 Preprint, astro-ph/9805201.

Seljak, U. & Zaldarriaga, M. 1996 *Astrophys. J.* **469**, 437.

Souradeep, T., Bond, J. R., Knox, L., Efstathiou, G. & Turner, M. S. 1998 Preprint, astro-ph/9802262.

TopHat home page. http://cobi.gsfc.nasa.gov/msam-tophat.html.

White, M., Carlstrom, J. E. & Dragovan, M. 1997 Preprint, astro-ph/9712195.

Zaldarriaga M., Spergel, D. & Seljak, U. 1997 Preprint, astro-ph/9702157.

PHILOSOPHICAL TRANSACTIONS OF THE ROYAL SOCIETY A MATHEMATICAL, PHYSICAL & ENGINEERING SCIENCES